Catalysis Today xxx (xxxx) xxx–xxx

Contents lists available at ScienceDirect

Catalysis Today

journal homepage: www.elsevier.com/locate/cattod

Investigation on hydroisomerization and hydrocracking of C_{15}–C_{18} *n*-alkanes utilizing a hollow tubular Ni-Mo/SAPO-11 catalyst with high selectivity of jet fuel

Guanhua Xing[a], Siyang Liu[a], Qingxin Guan[a,*], Wei Li[a,b,*]

[a] College of Chemistry, State Key Laboratory of Elemento-Organic Chemistry, Key Laboratory of Advanced Energy Materials Chemistry (Ministry of Education), Nankai University, Tianjin 300071, China

[b] Collaborative Innovation Center of Chemical Science and Engineering (Tianjin), Nankai University, Tianjin 300071, China

ARTICLE INFO

Keywords:
Jet fuel
Hydroisomerization
Hydrocracking
SAPO-11
Alkanes

ABSTRACT

This paper focused on the isomerization and cracking of *n*-alkanes to synthesize bio-jet fuel. A series of SAPO-11 supports with different Si/Al molar ratio (0.2, 0.4, 0.6) were prepared, characterized, and evaluated by the hydroisomerization on hydrodeoxygenation product of castor oil. As a result, a Ni-Mo/SAPO-11(0.4) catalyst with hollow tubular structure and moderate acidic strength exhibited optimum conversion (97.2%) and jet fuel selectivity (81.6%) in the reaction. Subsequently, Ni-Mo/SAPO-11(0.4) was selected to carry out further experiments on studying the hydroisomerization and hydrocracking of long chain *n*-alkanes. The results show that increasing temperature may promote hydroisomerization and hydrocracking. Temperature is more favorable for the reaction with the length of the carbon chain decreasing, no matter conversion, hydrocracking degree or isomerization tendency. The product selectivity of different *n*-alkanes is associated with the carbon number. In reaction to *n*-C_{18}, Ni-Mo/SAPO(0.4) surpassed the other two catalysts in the conversion and i/n ratio at 623 K which is the optimum temperature.

1. Introduction

In the recent years, biomass energy research has become a very cutting-edge research hotspot for its excellent application prospects on relieving the depletion of non-renewable energy and environmental pollution [1]. Jet fuel as the resource powering the aircraft engine, is becoming increasingly important in the transportation. The escalating demand for jet fuel takes up a big part in the worldwide transportation energy consumption [2]. Renewable bio-jet fuel could be produced by various routes, and the hydrogenation of vegetable oils has been proved to be the most viable route currently [3–8]. Nevertheless, it is still a significant challenge to achieve high selectivity and yield of jet fuel, and meanwhile satisfy the standard parameter like freezing point, cold flow and stability [9].

Two-step hydrogenation method is a common route to transform vegetable oils into hydrocarbons with high energy density and low oxygen content using bifunctional catalyst [5]. Hydrodeoxygenation (HDO) reaction is the first step, where vegetable oils were changed into alkanes by reactions like hydrogenation saturation, deoxygenation, decarbonylation, and decarboxylation. The second step is hydrocracking and hydroisomerization, where jet fuel range alkanes can be obtained. Common raw materials are vegetable oils extracted from oil crops like soybean, rapeseed, sunflower, castor, jatropha, camelina [7,10–15], or plants with high oil content like algae [16], and so on.

Hydroisomerization and hydrocracking have been widely studied, which are essential because they allow alkanes to meet the physicochemical testing criterion of combustion and other use [5,14]. For hydroisomerization and hydrocracking, various zeolites have been used as catalysts or supports to study [17–24]. However, there is not much research on hydroisomerization and hydrocracking for bio-jet fuel.

SAPO-11 is a kind of moderate acidic zeolite, which was frequently studied and employed as support in selective isomerization [25,26]. Verma et al. has reported they obtained about 40% diesel, 40% aviation kerosene, and remaining 20% being lighter gas range through investigating hydrogenation of jatropha oil over sulfide Ni-Mo and Ni-W supported on SAPO-11 with different Si content [15]. In our early studies, nonsulfide Ni supported on SAPO-11 were used as catalysts in the hydrogenation of castor oil [27]. However, there were heavy component in jet-fuel range products which indicated further

* Corresponding authors at: College of Chemistry, State Key Laboratory of Elemento-Organic Chemistry, Key Laboratory of Advanced Energy Materials Chemistry (Ministry of Education), Nankai University, Tianjin 300071, China.

E-mail addresses: qingxinguan@nankai.edu.cn (Q. Guan), weili@nankai.edu.cn (W. Li).

https://doi.org/10.1016/j.cattod.2018.04.028
Received 26 January 2018; Received in revised form 23 March 2018; Accepted 10 April 2018
0920-5861/ © 2018 Elsevier B.V. All rights reserved.

investigation on acidity adjustment of support. In this paper, SAPO-11 zeolites with different Si/Al molar ratio (0.2, 0.4, 0.6) were studied as catalyst support and tested using hydroisomerization and cracking of HDO products of castor oil. As a result, the ideal catalyst was sorted out and applied to carry out follow-up experiments.

Hydroisomerization on separate long chain alkanes is our further goal. Rossetti et al. [28] used Pt/SiO_2-Al_2O_3 catalyst to prove that both *n*-C_{16} and *n*-C_{28} conversion was affected by H_2/*n*-alkane ratio, and for C_{28} the influence was weaker, which was consistent with vapor liquid equilibrium data. The study on hydrotreatment of long-chain *n*-alkanes (i.e., *n*-C_{28}, *n*-C_{36}, and *n*-C_{44}), which was disposed in a stirred micro-autoclave via a 0.3% Pt/amorphous silica-alumina catalyst, showed that the conversion rate constants and iso-C_n lube and the iso-C_n nolube pseudocomponents selectivity were negatively correlated to the chain length, while reaction temperature had no obvious impact on the maximum yields [29]. Though many related isomerization experiments were executed [30–35], reactions on consecutive *n*-alkanes like C_{15}–C_{18} which can be widely obtained from HDO of vegetable oils [36] were rarely seen. Thus hydroisomerization and hydrocracking experiment of model compounds C_{15}–C_{18} was conducted to explore the regularity of the reaction.

2. Experimental

2.1. Materials

Pseudoboehmite ($AlOOH{\cdot}nH_2O$), 30 wt% acidic silica sol, nickel nitrate ($Ni(NO_3)_2{\cdot}6H_2O$) and ammonium molybdate ($(NH_3)_6Mo_7O_{24}{\cdot}4H_2O$) were purchased from Tianjin Guangfu Technology Development Co., Ltd. Phosphoric acid (H_3PO_4, 85 wt% in H_2O), dipropylamine (DPA) and diisopropylamine (DIPA) were brought from Shanghai Aladdin Bio-Chem Technology Co., Ltd. *n*-pentadecane, *n*-hexadecane, *n*-heptadecane, and *n*-octadecane (C_{15}–C_{18}, 99%) were purchased from Energy Chemical.

HDO product was acquired by HDO of castor oil which was reported previously [27]. It primarily composed of *n*-heptadecane, *n*-octadecane, certain *n*-alkanes with shorter chains, little i-alkanes, and remaining diluent cyclohexane. Some physicochemical properties of castor oil are listed in Table S1.

2.2. Catalysts preparation

A series of SAPO-11(x) zeolites with different Si/Al molar ratio (x = 0.2, 0.4, 0.6) were prepared by dynamic hydrothermal synthesis. At first, phosphoric acid was added into deionized water to form a solution. Then, pseudoboehmite was added into the solution and stirred for 2 h to make pseudoboehmite be completely dissolved. After that silica sol was added and stirred for 0.5 h. The next step was to introduce dipropylamine and diisopropylamine as template agent, and then the solution was stirred for 3 h. The molar ratio of different composition was 1.0 Al_2O_3 : 1.0 P_2O_5 : (0.6 DPA + 0.4 DIPA) : x SiO_2 : 92.5 H_2O, and x corresponds to different Si/Al molar ratio. And the mixture was fed into a 2 L autoclave and heated at 463 K for 24 h with a rotating speed of 200 r/min. Then the slurry was cooled to room temperature, centrifuged and washed three times with deionized water. The solid powder was dried at 383 K and calcined at 873 K for 6 h.

The catalyst was synthesized by incipient wetness impregnation method with nickel nitrate and ammonium molybdate aqueous solution. After that, the catalyst was dried at 383 K for 2 h and calcined at 773 K for 2 h in air atmosphere. Before the reaction the catalyst was reduced in hydrogen at 623 K in fixed bed reactor. The final prepared Ni-Mo catalyst involved 15.0 wt.% Ni and 5.0 wt.% Mo.

2.3. Catalysts characterization

Powder X-ray diffraction patterns (XRD) were measured by a Rigaku SmartLab high resolution X-ray diffractometer equipment with a Cu-Kα radiation source working at 45 kV and 200 mA. Scanning parameters included scanning angles (2θ range) from 5 to 90° and scanning rate at a speed of 8° min^{-1}. Field emission scanning electron microscope (SEM, JEOL, JSM-7500F) was operated to observe the morphology and particle size of the catalysts, which was assembled with energy-dispersive X-ray spectrometer (EDS). The samples were via gold spraying before placing on the sample table to refrain from charges accumulating and escalate the conductivity. Nitrogen adsorption desorption isotherms of samples at 77 K were performed on a BELSORP Max instrument. Untested samples went through a vacuum pretreatment at 423 K for 8 h first. Brunauer–Emmett–Teller (BET) model were applied to calculate the specific surface area. Pore volume and pore size distribution were estimated by nonlocal density functional theory (NLDFT) method. Temperature programmed reduction of H_2 (H_2-TPR) and temperature programmed desorption of NH_3 (NH_3-TPD) were carried out with a Micromeritics Chemisorb 2750 device. Prior to the experiment, all the samples were pretreated in a N_2 atmosphere at 573 K for 1 h. The reduction step was performed with 10 vol.% H_2/Ar gas mixture as the following program: from 298 K to 1073 K with a rate of 10 K min^{-1}. The desorption procedure was accomplished with a rate of 10 K min^{-1} from 323 K to 1073 K in Helium (25 mL min^{-1}).

2.4. Catalytic activity evaluation and products analysis

The prepared catalysts were pelleted, crushed, and screened out with 20–40 meshes. The feedstock was model compounds (C_{15}–C_{18}), which were diluted by cyclohexane with a constant mass ratio (1.5:1). All the reactions were conducted in a continuous flow fixed-bed reactor. Catalysts should be loaded in the constant temperature range directly without any dilution. The rest of reactor tube was packed with inert ceramic rings. The tests were all under a hydrogen pressure of 3 MPa and H_2/oil ratio of 800 with liquid hourly space velocity (LHSV) of 1 h^{-1}. The products were analyzed using Gas Chromatograph (Shimadzu, GC-2014, SH-Rtx-1 capillary column). Products composition analysis was acquired from GC–MS (Agilent 7890 A-5977C).

3. Results and discussion

3.1. Catalyst structure

The morphology of SAPO-11 with different silicon content are shown in Fig. 1. The particles of SAPO-11(0.4) are elongated aggregates of smaller particles and every independent particle exhibits a hollow tubular structure. It is different from SAPO-11(0.2) which was synthesized by static hydrothermal method [37]. When Si/Al molar ratio becomes 0.6, compared with SAPO-11(0.4), similar structure with larger size and more compact external surface emerges. This hollow porous structure may be more conducive to the diffusion of reactant molecules. TEM patterns of reduced catalyst are exhibited in Fig. S1. It can be concluded that metal particles are of even dispersion and particle size is around 20 nm.

The XRD patterns of different samples are shown in Fig. 2. The characteristic peaks at 8.1°, 9.4°, 13.1°, 15.6°, 20.3° and 21.1–23.2° demonstrate the typical SAPO-11 phase with AEL structure [38]. The intensity of peaks ranks in the following order: SAPO-11(0.4) > SAPO-11(0.2) > SAPO-11(0.6), which means SAPO-11(0.4) has relatively higher crystallinity [39]. Excessive Si content may bring a negative effect on the crystal growth and skeleton stability. The characteristic peaks show a tendency to shift to the left, indicating plane spacing becoming larger. The peaks at 2θ = 37.1°, 43.1°, 62.7°, and 75.3° reveal the existence of NiO.

As summarized in Table 1, with the increasing Si/Al molar ratio, specific surface area first reduces and then rises. Pore volume has a positive relation to the Si content. Specific surface area of all the samples decreased after impregnation due to metal component

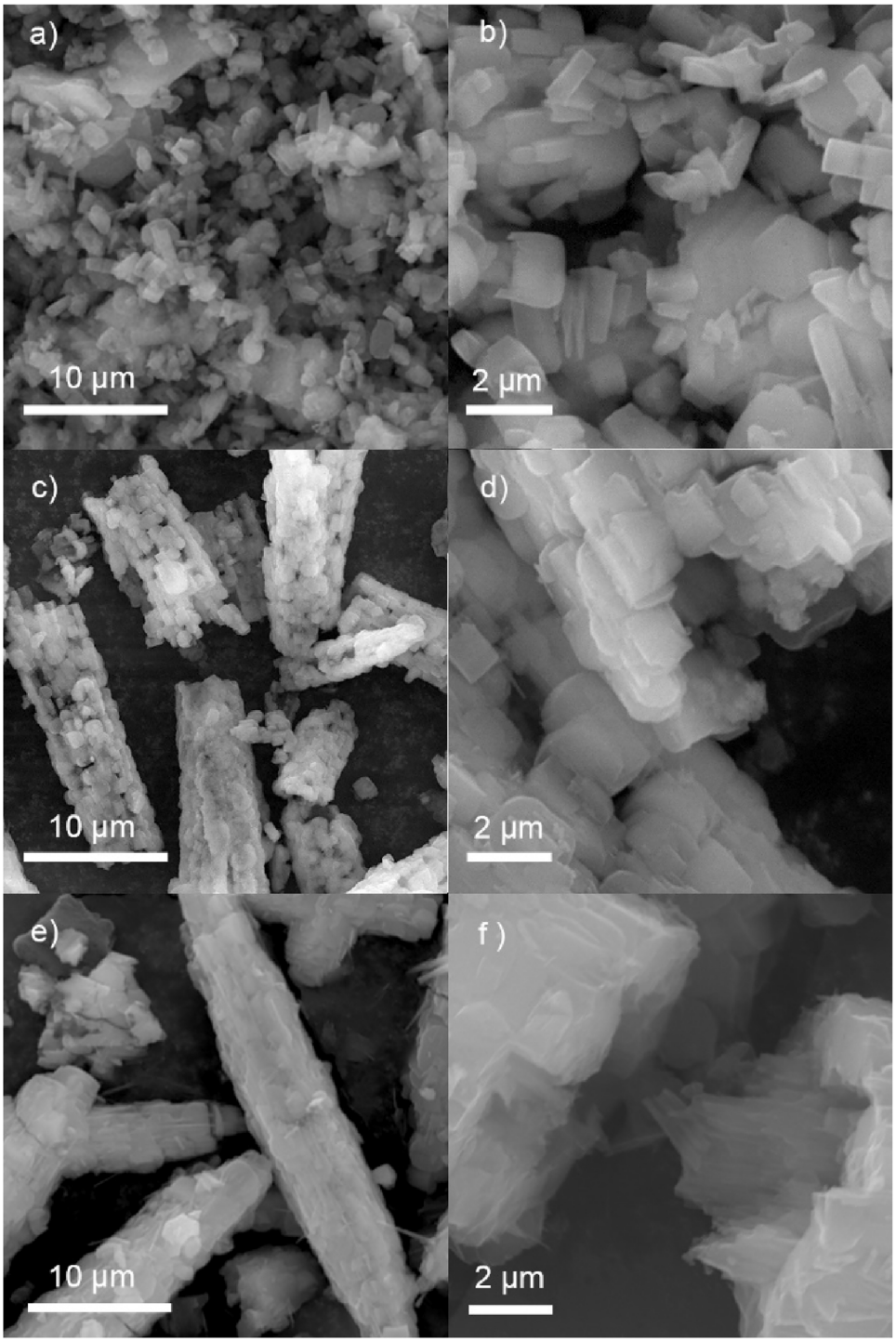

Fig. 1. SEM images of (a) and (b) SAPO-11(0.2), (c) and (d) SAPO-11(0.4), (e) and (f) SAPO-11(0.6).

introduction. According to N_2 adsorption-desorption isotherms in Fig.3, SAPO-11(0.2) exhibits type I isotherm which represents for microporous material. But isotherms of SAPO-11(0.4) and SAPO-11(0.6) are combined type I and type IV isotherm with a hysteresis loop [38], which implies a structure consisting of micropores and mesopores. This may be caused by homogeneous reaction at the dynamic stirring condition and inter-particle porosity formation [40].

NH_3-TPD results are presented in Fig. 4. All the curves have two peaks with temperature around 500 K and 600 K. To compare their relative acidity and strength, a Gaussian function was applied to do peak-differentiating and imitating with the two independent peaks recording as peak 1 and peak 2. Peak 1 and peak 2 correspond to weak and moderate acidic sites of SAPO-11. Respective results are summarized in Table S2. A left shift of the peak position with the Si/Al molar ratio increases, which demonstrates a decreasing tendency of acidity strength. When the Si/Al molar ratio increases, the peak area proportion also varies. SAPO-11(0.2) possesses a bit higher peak 1 and lower peak 2 than SAPO-11(0.4), which means it has more weak and less moderate acidic sites. SAPO-11(0.6) presents much higher peak 1 but lower peak 2 by contrast to SAPO-11(0.4), indicating it has more weak acidic sites and less moderate acidic sites. The evolution accompanied by the variation of Si/Al molar ratio shows that Si content has a crucial

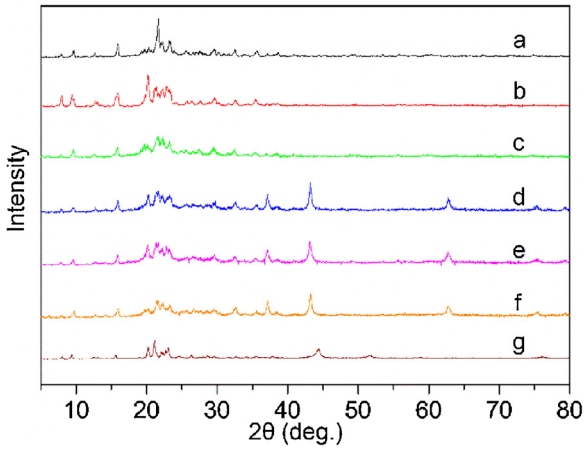

Fig. 2. XRD patterns of (a) SAPO-11(0.2); (b) SAPO-11(0.4); (c) SAPO-11(0.6); (d) Ni-Mo/SAPO-11(0.2); (e) Ni-Mo/SAPO-11(0.4); (f) Ni-Mo/SAPO-11(0.6); (g) spent Ni-Mo/SAPO-11(0.4).

Table 1
Surface properties of different samples.

Samples	S_{BET} ($m^2 g^{-1}$)	Total pore volume ($cm^3 g^{-1}$)
SAPO-11(0.2)	146	0.12
SAPO-11(0.4)	120	0.15
SAPO-11(0.6)	149	0.16
Ni-Mo/SAPO-11(0.2)	57.0	0.15
Ni-Mo/SAPO-11(0.4)	46.1	0.12
Ni-Mo/SAPO-11(0.6)	71.6	0.12

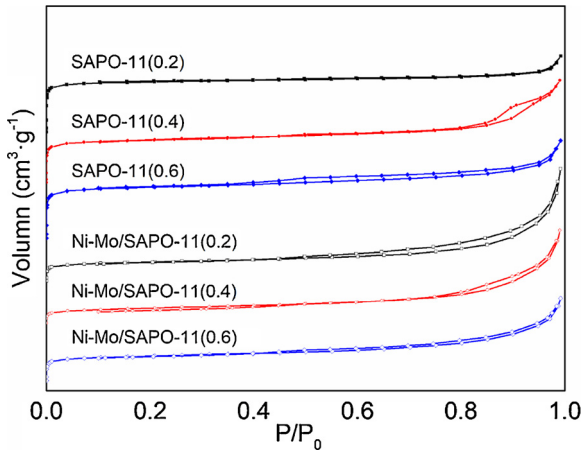

Fig. 3. N_2 adsorption-desorption isotherms of different samples.

effect on the strength and amounts of the acidic sites. The amount of framework silicon controls acidic property and excessive Si easily forms silicon islands adverse to acidic strength [38,41].

H_2-TPR results are shown in Fig. 4(d). It shows the reduction of Ni-Mo/SAPO-11(x) catalysts with different Si/Al molar ratio. The reduction peaks appear at two reduction temperature which are 832 K and 1048 K, respectively. The main peak is generated from the reduction of NiO ($Ni^{2+} \rightarrow Ni^{\circ}$) and partial reduction of MoO_3 ($Mo^{6+} \rightarrow Mo^{4+}$), while the second indistinct peak can be assigned to the complete reduction of Mo species [42].

3.2. Hydroisomerization and hydrocracking of HDO product

We started the trial on hydroisomerization and hydrocracking with different Ni-Mo/SAPO-11(x) catalysts. The HDO product of castor oil was used as feedstock, which was obtained through the method we have reported [27]. The analysis data are shown in Table 2. Some properties are exhibited in Table S3. The conversion here equals to a relative conversion which is based on the C_{17}–C_{18} consumption. Rel. Cov. = (1 − x/y) × 100%, x is corresponded to C_{17}–C_{18} selectivity of isomerization products and y refers to C_{17}–C_{18} component of the feedstock. All catalysts possess good activities and most of C_{17}–C_{18} alkanes were transformed into lighter alkanes. Ni-Mo/SAPO-11(0.4) achieves the highest conversion (97.2%). And for Ni-Mo/SAPO-11(0.2) and Ni-Mo/SAPO-11(0.6) are 96.3% and 92.0%, respectively. Thermogravimetric analysis (TGA) reveals a low coke content in all catalysts (shown in Fig. S2). Nonetheless, Ni-Mo/SAPO-11(0.4) was outstanding. The product selectivity of Ni-Mo/SAPO-11(0.4) for C_8–C_{16} (81.4%) is better than that of Ni-Mo/SAPO-11(0.2) (78.7% with many light products) and Ni-Mo/SAPO-11(0.6) (81.4% with many heavy products). According to the gas chromatograph results (shown in Fig. 5), the heavy component peaks, especially in which the retention time is 10.0–11.4 min (mainly C_{16}–C_{17}) in the patterns demonstrate weaker cracking activity of Ni-Mo/SAPO-11(0.6). While Ni-Mo/SAPO-11(0.2) and Ni-Mo/SAPO-11(0.4) show better effect by the even distribution, signifying moderate hydroisomerization accomplished coupling with hydrocracking. Ni-Mo/SAPO-11(0.4) catalyst shows higher cracking degree and optimal selectivity of jet fuel range alkanes. This result agrees well with the NH_3-TPD result. Meanwhile, there is no obvious distinction in XRD pattern between fresh Ni-Mo/SAPO-11(0.4) and spent Ni-Mo/SAPO-11(0.4) (shown in Fig. 2). Therefore, Ni-Mo/SAPO-11(0.4) was chosen to test in hydroisomerization and hydrocracking of C_{15}–C_{18} *n*-alkane model compounds.

3.3. Hydroisomerization and hydrocracking of C_{15}–C_{18} n-alkanes

A series of experiments were carried out under 3 MPa and H_2/oil ratio of 800:1 at a temperature gradient (583, 603, and 623 K). The conversion is calculated by detecting how much *n*-C_m (m refers to the carbon number of the feedstock *n*-alkane) was translated including hydroisomerization and hydrocracking, and the data are listed in Table 3. It can be concluded that high temperature (623 K) makes a huge contribution in increasing conversion (almost to 100%). Apart from optimum acidic strength, we hypothesize that high activity may result from the mesoporous structures of SAPO-11(0.4). It may help alkanes to get sufficient contact with well-dispersed active sites and achieve satisfactory catalytic effect. It can be deduced that short chain *n*-alkane conversion is susceptible to the temperature according to the curves. For *n*-C_{15}, when temperature increased from 583 K to 623 K, conversion rate almost double increased. At all temperature conditions *n*-C_{18} presents the highest conversion, which means longer chain of *n*-alkane is more easily to be transformed. The overall product isomer/*n*-alkane (i/n) ratios are also listed in Table 3. Temperature has a positive effect on the isomerization of alkanes, which is more obvious for long-chain alkanes.

Fig. 6 shows the ratio of isomer/*n*-alkane (i/n) and the selectivity of the products. The ratio of i/n increases accompanied with the carbon number increasing. At low temperature, the curves are similar including the relative minimum value at C_{12}. The similarity may be caused by the low isomerization activity for all *n*-alkanes, though *n*-C_{18} shows higher overall ratio. All the ratios increase sharply when raising the reaction temperature. At high temperature, strong hydrocracking effect leads to less long chain products and weaker hydroisomerization tendency. As a result, the latter half curves decline. The reason why high ratio of product C_{17} of feedstock n-C_{18} emerges (Fig. 6a) is that the lower content of C_{17} selectivity according to Fig. 5d. It can be concluded that the product of C_{17} coming from *n*-C_{18} cracks easier than other C_{m-1} coming from *n*-C_m at high temperature (623 K). The distinction of different *n*-alkanes is that short chain *n*-alkanes are more sensitive to the temperature change, such as the upper and lower order of the curves are completely reversed at 583 K and 623 K.

Furthermore, high temperature leads to intense cracking and

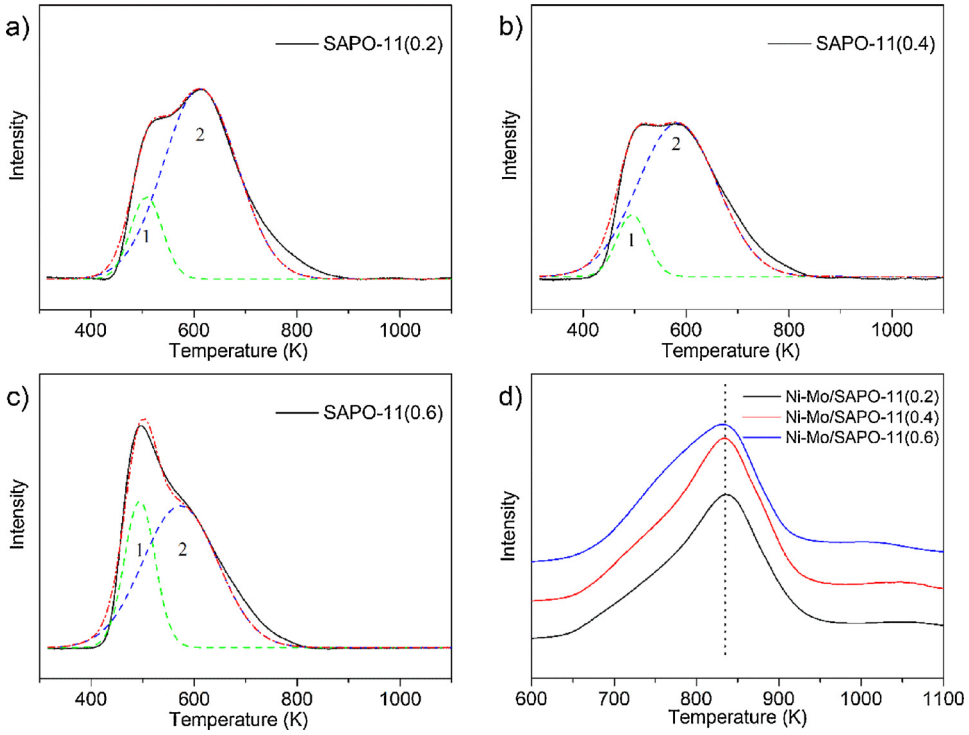

Fig. 4. NH_3-TPD patterns (a–c) of SAPO-11(x) supports, and H_2-TPR patterns (d) of different Ni-Mo/SAPO-11(x) catalysts.

Table 2
GC analysis of the reaction products with different catalysts at 623 K.

Samples	Selectivity (%)		
	C_5–C_7	C_8–C_{16}	C_{17}–C_{18}
HDO product	3.9	11.6	84.5
Ni-Mo/SAPO-11(0.2)	18.2	78.7	3.1
Ni-Mo/SAPO-11(0.4)	16.2	81.4	2.4
Ni-Mo/SAPO-11(0.6)	16.9	76.3	6.8

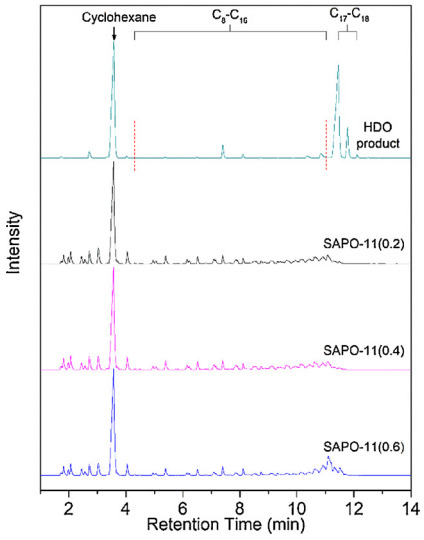

Fig. 5. The GC analysis patterns of products at 623 K.

obtains light products of even distribution with less heavy products. Low temperature weakens cracking degree visibly and products of long carbon chain become dominant. Temperature has a strong effect on hydrocracking of short chain *n*-alkane. For example, light products

Table 3
Results of the isomerization of C_{15}–C_{18} *n*-alkanes using Ni-Mo/SAPO-11(0.4).

Feedstock	Temperature (K)	Conversion (%)	Ratio (i/n)
n-C_{15}	623	99.86	2.47
n-C_{15}	603	93.18	1.33
n-C_{15}	583	51.39	0.38
n-C_{16}	623	99.84	2.59
n-C_{16}	603	96.02	1.37
n-C_{16}	583	63.19	0.53
n-C_{17}	623	99.88	2.54
n-C_{17}	603	96.21	1.49
n-C_{17}	583	68.91	0.75
n-C_{18}	623	99.97	2.74
n-C_{18}	603	96.70	1.69
n-C_{18}	583	73.89	0.59

(such as C_8–C_{12}) selectivity of *n*-C_{15} at 623 K is larger than other *n*-alkanes while at low temperature they are nearly the same. For different feedstock *n*-alkanes at the same temperature, it's very similar that the selectivity of different product approximately increases along with its carbon number. It indicates that no specific cracking position or tendency among the carbon chain when the cracking reaction occurs at active sites. The curves show a similar shape at the same temperature and a connection with the carbon number of *n*-C_m. For example, at 603 K, the relative maximum value of *n*-C_{15} emerges at C_{14}, for *n*-C_{16} at C_{15}, for *n*-C_{17} at C_{16}, and for *n*-C_{18} at C_{17}. It indicates that at low temperature length of carbon chain plays a vital role in the product distribution. It can be concluded that low temperature will result in cracking at terminal C—C bond, while high temperature will result in cracking step by step to produce light products. So far, the above results show that hydroisomerization and hydrocracking are competitive mechanism which originates from the reaction essence [43].

We summarized the ratio of i/n of C_m itself (m = 15, 16, 17, 18, refer to carbon number) which was not talked about above to find out the change rule of i-C_m product component (as shown in Fig. 7). The selectivity increases along with the raising temperature, which is similar to the overall i/n ratio. But at different temperature, the variation

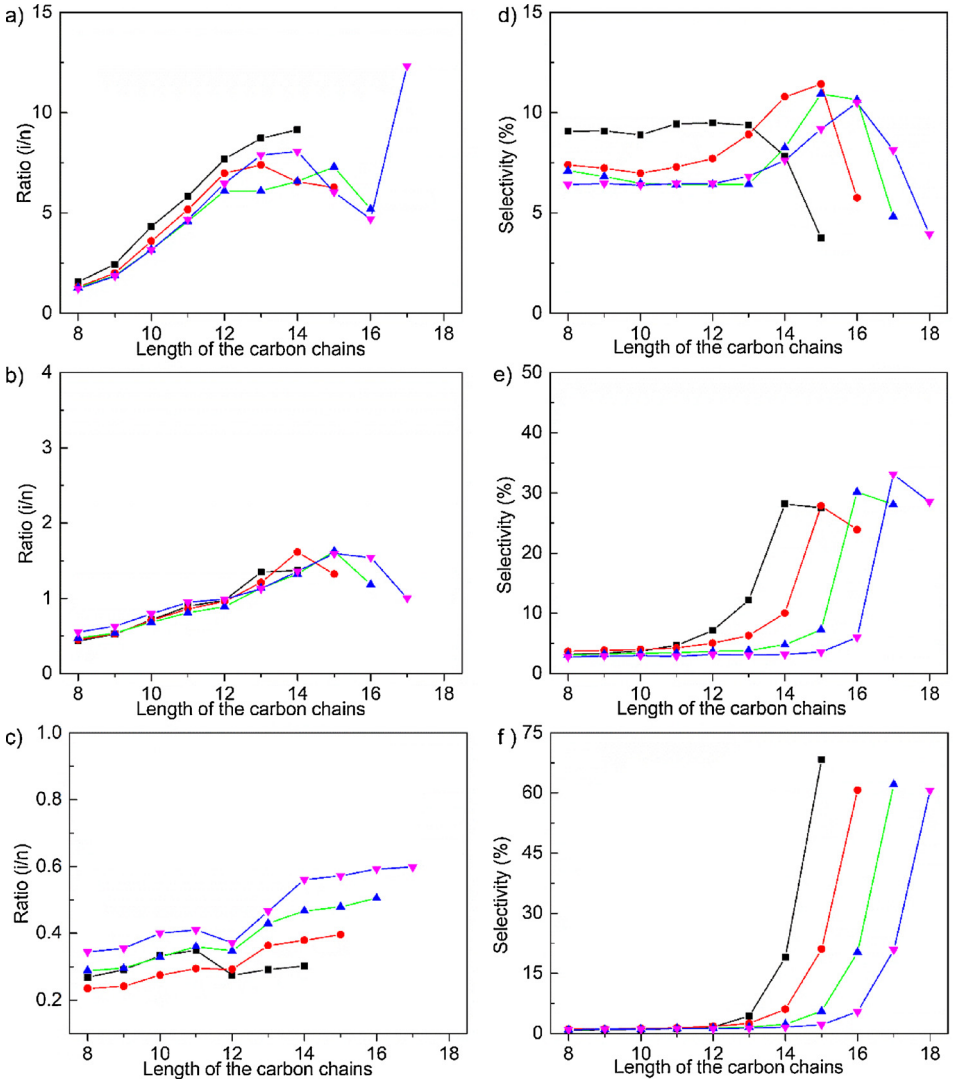

Fig. 6. The ratio of isomer/*n*-alkane (i/n) and the selectivity at different temperatures: (a) and (d) at 623 K, (b) and (e) at 603 K, (c) and (f) at 583 K. The symbols represent for different feedstock: *n*-C_{15} (-■-), *n*-C_{16} (-●-), *n*-C_{17} (-▲-), *n*-C_{18} (-▼-).

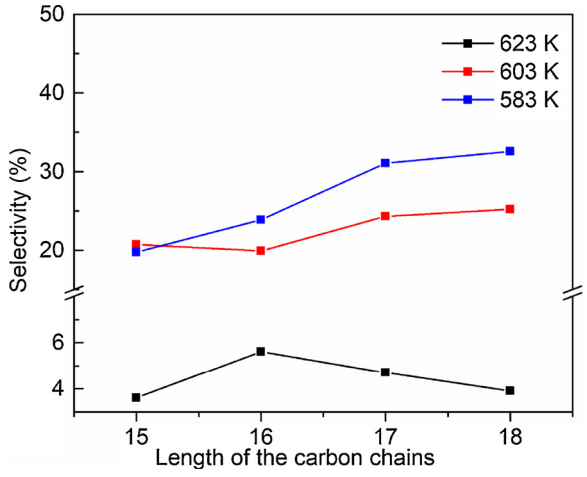

Fig. 7. The selectivity of isomer of C_m at different temperatures.

tendency of the curve is not the same. At low temperature (583 K and 603 K), long carbon chain is more likely to isomerize. Nevertheless, when the temperature increased the curve inclination varied. *n*-C_{16} shows the highest activity of self-isomerization, while i-C_{17} and i-C_{18} diminish clearly. The explanation is that a high temperature leads to strong cracking of carbon chain and weakens hydroisomerization caused by transfer of carbocation. It verifies the competitive mechanism existing between hydroisomerization and hydrocracking as well.

3.4. Hydroisomerization and hydrocracking of n-C_{18} with different catalysts

Catalysts with different Si/Al molar ratio were probed further after the investigation on C_{15}–C_{18} *n*-alkanes. C_{18} served as the feedstock and similar hydroisomerization and hydrocracking reaction was designed. Results are summarized in Fig. 8 and product data are listed in Table S4. Ni-Mo/SAPO(0.4) remains the superiority in conversion and i/n ratio. At 623 K, Ni-Mo/SAPO(0.4) has the maximum selectivity of C_8–C_{16} alkanes (Table S4) which agrees well with the reaction on HDO products (Table 2). However, low temperature impairs its hydrocracking activity obviously and leads to low selectivity close to Ni-Mo/SAPO (0.2) and Ni-Mo/SAPO(0.6) or even worse (shown in Fig. 8). As a result, Ni-Mo/SAPO(0.4) exhibits better performance at 623 K which is the optimum temperature for the reaction.

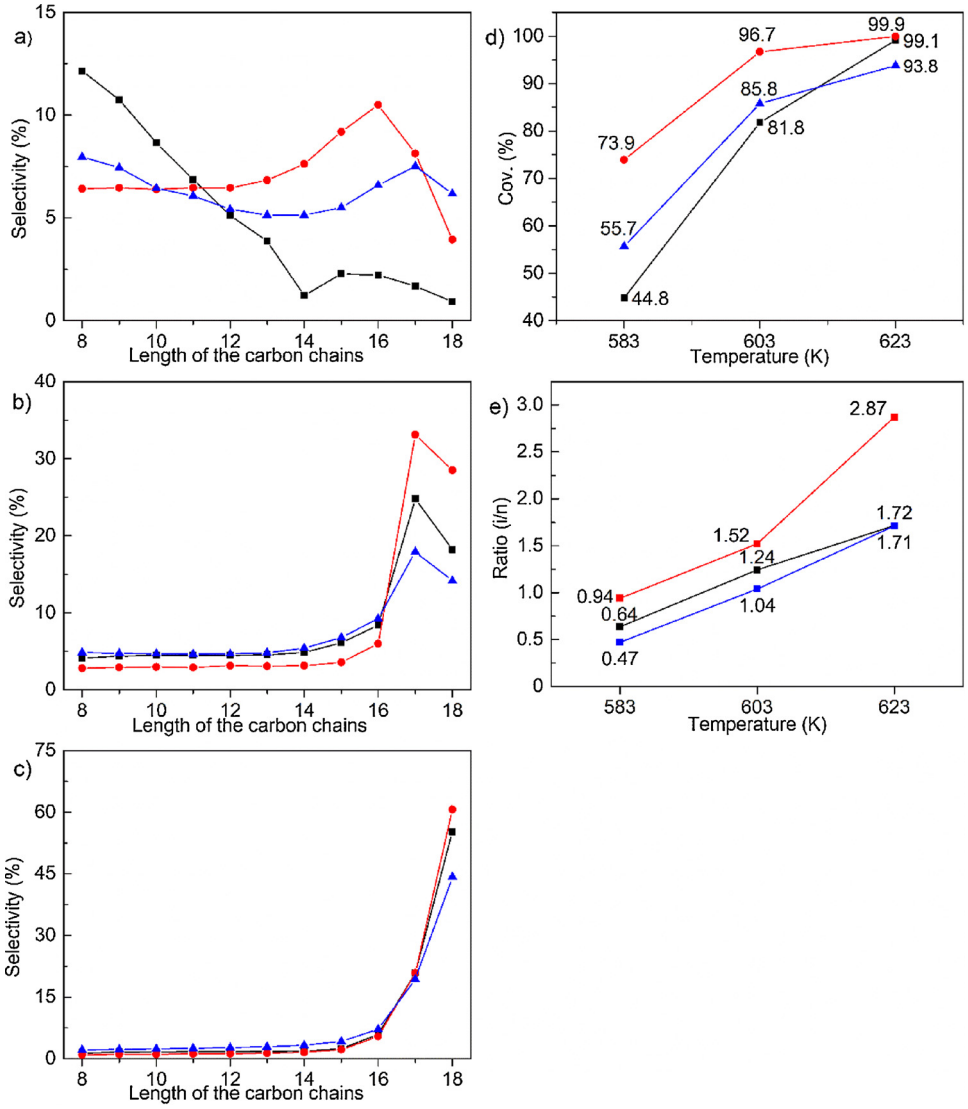

Fig. 8. Reaction results of *n*-C_{18}. (a), (b) and (c): product selectivity at different reaction temperature which is 623 K, 603 K and 583 K, respectively. The conversion and ratio of isomer/n-alkane (i/n) with different catalysts at different temperatures are charted separately in (d) and (e). The symbols represent different catalyst: Ni-Mo/SAPO-11(0.2) (-■-), Ni-Mo/SAPO-11(0.4) (-●-), Ni-Mo/SAPO-11(0.6) (-▲-).

4. Conclusions

This paper studied the isomerization and cracking of *n*-alkanes to synthesize bio-jet fuel. A series of SAPO-11 zeolite supports with different Si/Al molar ratio (0.2, 0.4, 0.6) were synthesized, which were characterized using SEM, XRD, NH_3-TPD, H_2-TPR, and further evaluated by the hydroisomerization on HDO product of castor oil after uploading Ni-Mo in a fix-bed reactor. As a result, a Ni-Mo/SAPO-11(0.4) catalyst with hollow tubular structure and moderate acidic strength exhibited optimum conversion (97.2%) and jet fuel selectivity (81.6%). Subsequently, Ni-Mo/SAPO-11(0.4) was selected to carry out further experiments on studying the hydroisomerization and hydrocracking of long chain *n*-alkanes (C_{15}–C_{18}). The results show that increasing temperature from 583 K to 623 K may promote hydroisomerization and hydrocracking. Temperature is more favorable for the reaction with the length of the carbon chain decreasing, no matter conversion, hydrocracking degree or isomerization tendency. Long chain *n*-alkanes show favorable performance at low temperature while short chain *n*-alkanes are on the contrary. The product selectivity of different *n*-alkanes is associated with the carbon number. Strong hydrocracking is not conducive to the self-isomerization of *n*-alkane. At last, in reaction on *n*-C_{18}, Ni-Mo/SAPO(0.4) surpassed the other two catalysts in conversion and i/n ratio and 623 K is the optimum temperature.

Acknowledgements

This work was financially supported by the NSFC (21603107, 21376123, U1403293), MOE (IRT-13R30 and 113016A), NSFT (15JCQNJC05500, 16YFZCGX00020), and the Research Fund for 111 Project (B12015).

Appendix A. Supplementary data

Supplementary material related to this article can be found, in the online version, at doi:https://doi.org/10.1016/j.cattod.2018.04.028.

References

[1] R. Mawhood, E. Gazis, S. de Jong, R. Hoefnagels, R. Slade, Biofuel Bioprod. Biorefin. 10 (2016) 462–484.
[2] I.A.T. Association, IATA Air Passenger Forecast Shows Dip in Long-Term Demand, (2015).

[3] S. Karatzos, J.S. van Dyk, J.D. McMillan, J. Saddler, Biofuel Bioprod. Biorefin. 11 (2017) 344–362.
[4] D. Chiaramonti, M. Prussi, M. Buffi, D. Tacconi, Appl. Energy 136 (2014) 767–774.
[5] A. Galadima, O. Muraza, J. Ind. Eng. Chem. 29 (2015) 12–23.
[6] Z. Eller, Z. Varga, J. Hancsók, Fuel 182 (2016) 713–720.
[7] A. Llamas, A.-M. Al-Lal, M. Hernandez, M. Lapuerta, L. Canoira, Energy Fuel 26 (2012) 5968–5976.
[8] A. Llamas, M.J. García-Martínez, A.-M. Al-Lal, L. Canoira, M. Lapuerta, Fuel 102 (2012) 483–490.
[9] T.K. Hari, Z. Yaakob, N.N. Binitha, Renew. Sust. Energy Rev. 42 (2015) 1234–1244.
[10] J. Duan, J. Han, H. Sun, P. Chen, H. Lou, X. Zheng, Catal. Commun. 17 (2012) 76–80.
[11] S.K. Kim, S. Brand, H.-S. Lee, Y. Kim, J. Kim, Chem. Eng. J. 228 (2013) 114–123.
[12] H. Wang, S. Yan, S.O. Salley, K.Y.S. Ng, Ind. Eng. Chem. Res. 51 (2012) 10066–10073.
[13] J. Horáček, Z. Tišler, V. Rubáš, D. Kubička, Fuel 121 (2014) 57–64.
[14] M.C. Vasquez, E.E. Silva, E.F. Castillo, Biomass Bioenergy 105 (2017) 197–206.
[15] D. Verma, B.S. Rana, R. Kumar, M.G. Sibi, A.K. Sinha, Appl. Catal. A-Gen. 490 (2015) 108–116.
[16] A. Cole, Y. Dinburg, B.S. Haynes, Y. He, M. Herskowitz, C. Jazrawi, M. Landau, X. Liang, M. Magnusson, T. Maschmeyer, A.F. Masters, N. Meiri, N. Neveux, R. de Nys, N. Paul, M. Rabaev, R. Vidruk-Nehemya, A.K.L. Yuen, Energy Environ. Sci. 9 (2016) 1828–1840.
[17] A. Galadima, O. Muraza, Int. J. Energy Res. 39 (2015) 741–759.
[18] C. Gutierrez-Antonio, F.I. Gomez-Castro, J.A. de Lira-Flores, S. Hernandez, Renew. Sust. Energy Rev. 79 (2017) 709–729.
[19] R. Buzzoni, S. Bordiga, G. Ricchiardi, C. Lamberti, A. Zecchina, G. Bellussi, Langmuir 12 (1996) 930–940.
[20] E.Y. Emori, F.H. Hirashima, C.H. Zandonai, C.A. Ortiz-Bravo, N.R.C. Fernandes-Machado, M.H.N. Olsen-Scaliante, Catal. Today 279 (2017) 168–176.
[21] P. Lanzafame, S. Perathoner, G. Centi, E. Heracleous, E.F. Iliopoulou, K.S. Triantafyllidis, A.A. Lappas, ChemCatChem 9 (2017) 1632–1640.
[22] J. Cheng, T. Li, R. Huang, J. Zhou, K. Cen, Bioresour. Technol. 158 (2014) 378–382.
[23] J. Hancsók, M. Krár, S. Magyar, L. Boda, A. Holló, D. Kalló, Stud. Surf. Sci. Catal. 170 (2007) 1605–1610.
[24] J. Hancsók, Z. Eller, G. Pölczmann, Z. Varga, A. Holló, G. Varga, Clean Technol. Environ. 16 (2014) 1445–1454.
[25] T. Blasco, A. Chica, A. Corma, W.J. Murphy, J. Agúndez-Rodríguez, J. Pérez-Pariente, J. Catal. 242 (2006) 153–161.
[26] A.K. Sinha, S. Sivasanker, Catal. Today 49 (1999) 293–302.
[27] S. Liu, Q. Zhu, Q. Guan, L. He, W. Li, Bioresour. Technol. 183 (2015) 93–100.
[28] I. Rossetti, C. Gambaro, V. Calemma, Chem. Eng. J. 154 (2009) 295–301.
[29] V. Calemma, S. Peratello, F. Stroppa, R. Giardino, C. Perego, Ind. Eng. Chem. Res. 43 (2004) 934–940.
[30] F. Bauer, K. Ficht, M. Bertmer, W.-D. Einicke, T. Kuchling, R. Glaeser, Catal. Sci. Technol. 4 (2014) 4045–4054.
[31] V.A. Benitez, J.C. Yori, J.A. Grau, C.L. Pieck, C.R. Vera, Energy Fuel 20 (2006) 422–426.
[32] J. Kang, W. Ma, R.A. Keogh, W.D. Shafer, G. Jacobs, B.H. Davis, Catal. Lett. 142 (2012) 1295–1305.
[33] L.C. Gomes, D.D.O. Rosas, R.C. Chistone, F.M. Zanon Zotin, L.R. Raddi de Araujo, J.L. Zotin, Fuel 209 (2017) 521–528.
[34] A.H. Thaker, M. John, K. Kumar, M.W. Kasture, S. Parmar, B.L. Newalkar, P.A. Parikh, Int. J. Chem. React. Eng. 14 (2016) 155–165.
[35] S. Parmar, K.K. Pant, M. John, K. Kumar, S.M. Pai, B.L. Newalkar, Energy Fuel 29 (2015) 1066–1075.
[36] E. Furimsky, Catal. Today 217 (2013) 13–56.
[37] M. Höchtl, A. Jentys, H. Vinek, Catal. Today 65 (2001) 171–177.
[38] X. Cui, Y. Liu, X. Liu, Catal. Lett. 145 (2015) 1464–1473.
[39] S. Zhang, S.-L. Chen, P. Dong, G. Yuan, K. Xu, Appl. Catal. A-Gen 332 (2007) 46–55.
[40] H. Xu, J. Guan, S. Wu, Q. Kan, J. Colloid Interface Sci. 329 (2009) 346–350.
[41] X. Wang, F. Guo, X. Wei, Z. Liu, W. Zhang, S. Guo, L. Zhao, Korean J. Chem. Eng. 33 (2016) 2034–2041.
[42] L. Qu, W. Zhang, P.J. Kooyman, R. Prins, J. Catal. 215 (2003) 7–13.
[43] H.L. Coonradt, W.E. Garwood, Ind. Eng. Chem. Process Des. Dev. 3 (1964) 38–45.